Jour. Korean Inst. Mining Geol.
V. 17, No. 1, 1984 p. 49—55

Analyses of Dipole-Dipole IP Responses over Dipping Structures

Hee Joon Kim*

Abstract: This paper describes three-dimensional (3-D) standard curves for conductive dipping buried bodies in induced polarization (IP) method. Dipole-dipole IP responses for the dipping bodies are calculated by the numerical modeling technique using an integral equation solution. Dip angles of the bodies are 0, 20, 45, 70 and 90 degrees, respectively.

The horizontal (0-degree dip) and vertical (90-degree dip) bodies produce symmetrical patterns of IP responses. The dipping bodies of 20, 45 and 70 degrees, however, produce asymmertical patterns, with the highest IP contours dipping in the direction opposite to the bodies in pseudo-sections. The most remarkable asymmetrical pattern appears in the model of 20-degree dip. It is difficult to distinguish the body of 70-degree dip from that of 90-degree dip on the basis of dipole-dipole IP data. The IP pattern in pseudo-sections varies when the line moves away from the center of the body along strike, with the anomaly deeper and smaller in amplitude. IP maps seem to be more useful than IP pseudo-sections in predicting the location of target.

Introduction

Electromagnetic (EM) coupling is one of serious ploblems in IP surverying. In order to reduce the EM coupling easily, dipole-dipole array is frequently used in IP surveying. Besides it usually gives the largest anomalies compared with other arrays and has best overall resolution. However it is known that this array has poor resolution for a dipping structure (Coggon, 1973). Pelton et al. (1978), therefore, excludes purposely the dip of target from model parameters in his two-dimensional (2-D) inversion technique.

Numerical modeling techniques enable us to evaluate systematically the effects of a number of different model parameters. The numerical modeling technique using an integral equation solution is one of the most cost-effective one for simple 3-D models (Hohmann, 1975; Endo et al., 1979; Pridmore et al., 1981). Kim (1983) showed the effects of changes in six model parameters (width, strike length, depth extent, depth, body position along line and line position along strike) on the IP responses of conductive prismatic bodies. In this paper we show the effect of dip on the dipole-dipole IP responses of conductive bodies.

In order to analyze the effect of dip, dip angles of the bodies are taken as 0, 20, 45, 70 and 90 degrees, respectively. The IP responses over the dipping structures are illustrated not only by pseudo-sections at each line but also by maps at each dipole separation. These IP standard curves are calculated by the 3-D integral equation method (Kim, 1983).

Models

In the integral equation method, unknown potentials must be found only in anomalous bodies. Thus the body is divided into a number of cubic cells in numerical calculations. In this study we consider five models which have a single inhomogeneity, and each body is divided into forty cubic cells.

The model parameter is the dip angles of the

* Department of Applied Geology, National Fisheries University of Pusan, Pusan 608, Korea

bodies: 0, 20, 45, 70 and 90 degrees. It is easy to model a dipping body by displacing the cubic cells into which it is divided. As an example of models the 20-degree dipping structure is shown in Fig. 1. The earth except for the body having resistivity ρ_2 is taken to be a half-space of resistivity ρ_1. The ratio of the body resistivity to the earth resistivity is fixed to $\rho_2/\rho_1=3.0/12.5$ in all models.

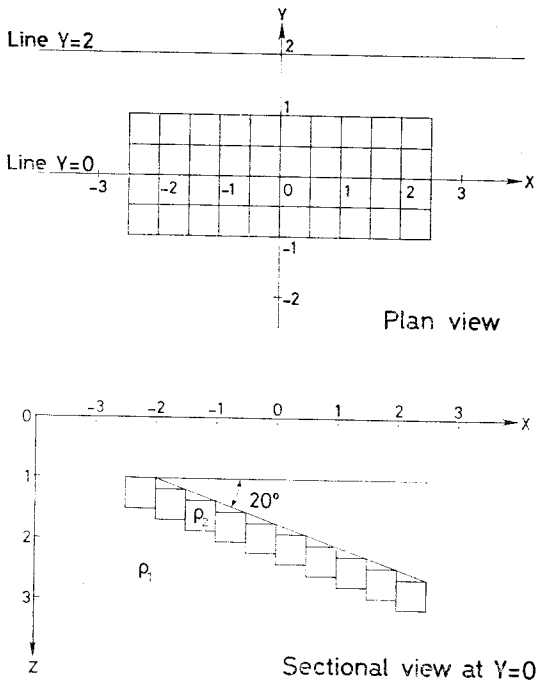

Fig. 1 Plan and sectional views of the 20-degree dipping structure. The earth excpt for the body having resistivity ρ_2 is taken to be a half-space of resistivity ρ_1. All dimensions are in units of dipole length.

As usuall, all dimensions are in units of dipole length. In all models the depth to the top of body is 1 unit, the strike length is 2 units and the size of each cubic cell is $0.5\times0.5\times0.5$ units. The total width and thickness of body, of course, vary with the dip angles.

Numerical results

Numerical results are obtained along each parallel line normal to strike. These results are shown in both pseudo-sections and maps. The pseudo-sections are illustrated for two lines (see Fig. 1): at the center line of the body bisecting the strike (Y=0) and at the line of one unit off end of the body (Y =2).

0-degree dip

Fig. 2 shows IP pseudo-sections over the horizontal structure of 0 degree. The width and thickness of body are 5 and 0.5 units, respectively.

In the pseudo-section at Y=0, the highest IP response over 16% occurs directly below the body. The high anomaly associated with the body shows

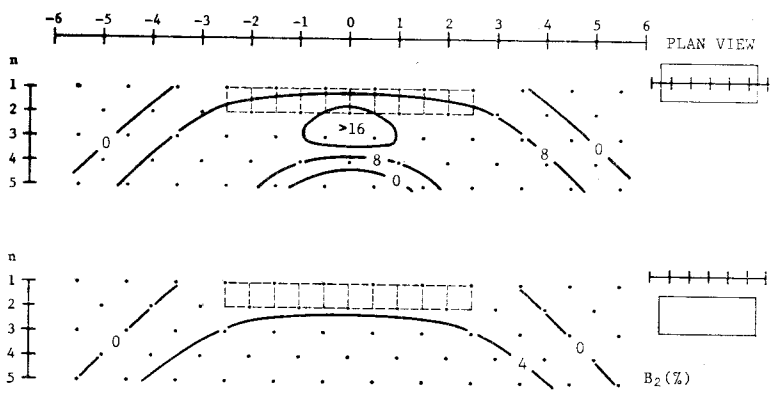

Fig. 2 IP pseudo-sections for the horizontal structure along lines Y=0 (upper) and Y=2 (lower). The width of body is 5 units, the strike length 2, the thickness 0.5, the depth 1 and the resistivity ratio $\rho_2/\rho_1=3.0/12.5$.

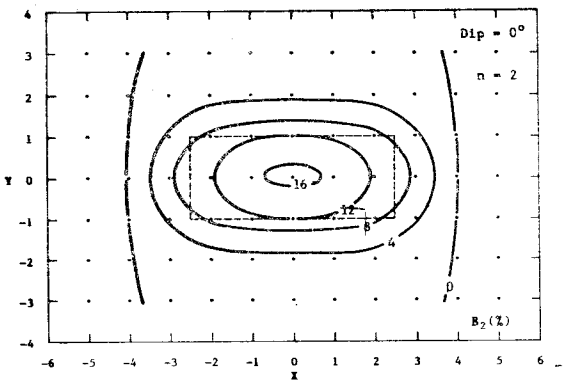

Fig. 3 IP map for the horizontal structure at n=2. The model is the same as in Fig. 2.

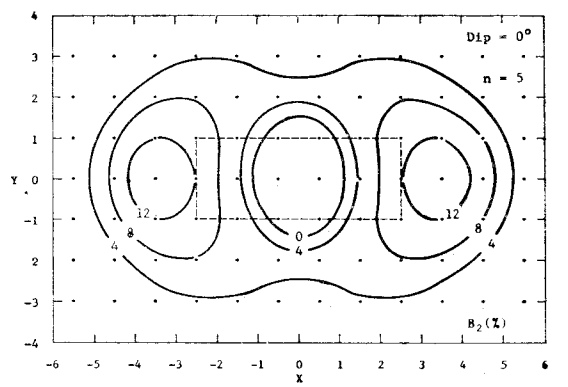

Fig. 4 IP map for the horizontal structure at n=5. The model is the same as in Fig. 2.

a sharp drop in amplitude with moving the line away from the center of body. In the pseudo-section at Y=2, broad and low anomalies appear below the body at large dipole separations. Since the dipole-dipole array is symmetrical, the horizontal structure produces symmetrical patterns of IP responses.

Figs. 3 and 4 show IP maps over the horizontal structure. In the map at two units of dipole separation (n=2, Fig. 3), elliptical contours are observed at the location of body. The IP patterns of n=1 and 3 are similar to that of n=2. In the map at five units of dipole separation (n=5, Fig. 4), however, high anomalies appear separately at the both end-sides of body, and the negative anomaly appears at the central part of body. The pattern of n=4 is similar to that of n=5, but the negative value does not appear.

20-degree dip

Fig. 5 shows IP pseudo-sections over the 20-degree dipping structure. The total width and thickness of body are 5 and about 2.14 units, respectively.

The most remarkable feature in the dipping structure is the asymmetrical pattern of IP responses in the pseudo-section. In the pseudo-sec

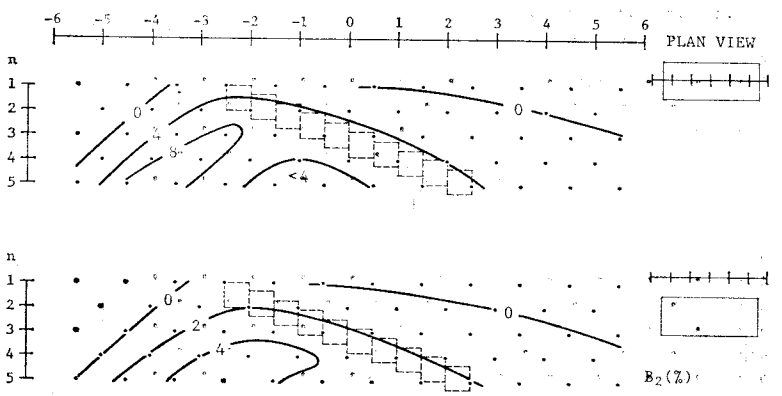

Fig. 5 IP pseudo-sections for the 20-degree dipping structure along lines Y=0 (upper) and Y=2 (lower). The total width of body is 5 units, the strike length 2, the total thickess about 2.14, the depth 1 and the resistivity ratio ρ_2/ρ_1=3.0/12.5.

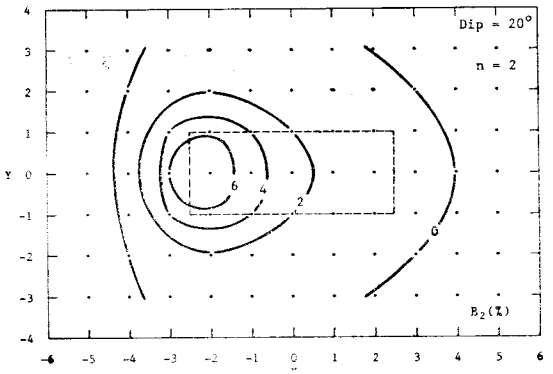

Fig. 6 IP map for the 20-degree dipping structure at n=2. The model is the same as in Fig. 5.

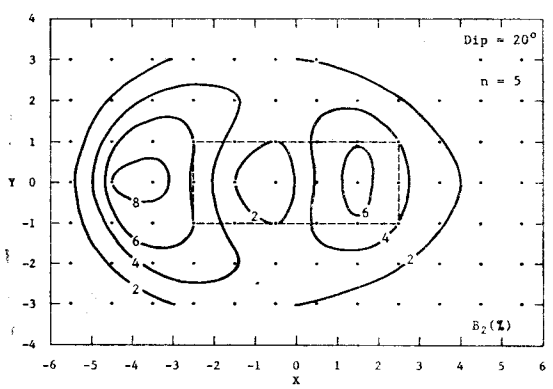

Fig. 7 IP map for the 20-degree dipping structure at n=5. The model is the same as in Fig. 5.

tion at Y=0, the highest contour of 8% appears on the side oppsite to the direction of dip. The basic pattern is maintained but anomalies at Y=2 decrease to about half.

Figs. 6 and 7 show IP maps at n=2 and 5 over the 20-degree dipping structure. In Fig. 6 (n=2), the highest anomaly is observed at the up-dip end of the body. In Fig. 7 (n=5), although the highest anomaly over 8% is observed at the up-dip side, another high anomaly over 6% appears at the down-dip side. This is almost the same tendency as the response of the horizontal structure at n =5, but the negative value is not observed at the location of body.

45-degree dip

Fig. 8 shows IP pseudo-sections over the 45-degree dipping structure. The total width and thickness of body are 4 and 3.75 units, respectively.

In the pseudo-section at Y=0, the highgest IP response over 6% appears on the side opposite to the direction of dip. This asymmetrical pattern is almost the same tendency as the 20-degree dip (Fig. 5). The asymmetrical pattern, however, is lost at Y=2, and nearly symmetrical contours are observed.

Fig. 9 shows an IP map at n=3 over the 45-

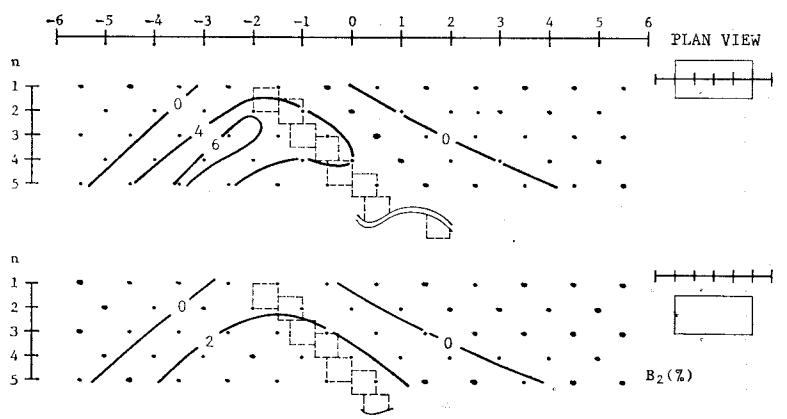

Fig. 8 IP pseudo-sections for the 45-degree dipping structure along lines Y=0 (upper) and Y=2 (lower). The total width of body is 4 units, the strike length 2, the total thickness 3.75, the depth 1 and the resistivity ratio ρ_2/ρ_1=3.0/12.5.

degree dipping structure. The highest anomaly is observed at the up-dip end of the body. In the case of 45-degree dip, IP maps at n=1 to 5 show nearly same patterns.

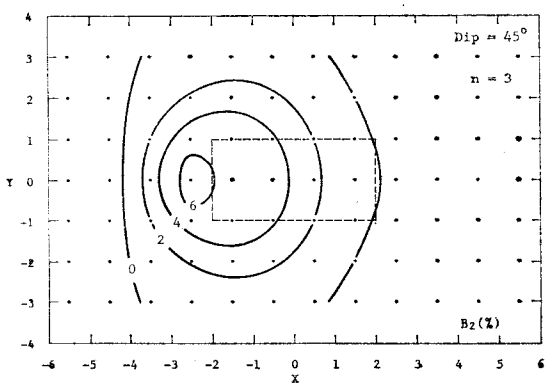

Fig. 9 IP map for the 45-degree dipping structure at n=3. The model is the same as in Fig. 8.

70-degree dip

Fig. 10 shows IP pseudo-sections over the 70-degree dipping structure. The total width and thickness of body are about 2.14 and 5 units, respectively.

In the pseudo-section at Y=0, only the highest contour of 6% is slightly asymmetrical, and the other contours are nearly symmetrical. These symmetrical patterns will be expected to be more marked at the other lines. In fact the asymmetrical pattern is lost almost completely at Y=2.

Fig. 11 shows an IP map at n=3 over the 70-degree dipping structure. Circular contours centered at the up-dip end of the body are observed. It is difficult to distinguish the 70-degree dipping body from the vertical body on the basis of the IP pattern (see Fig. 13).

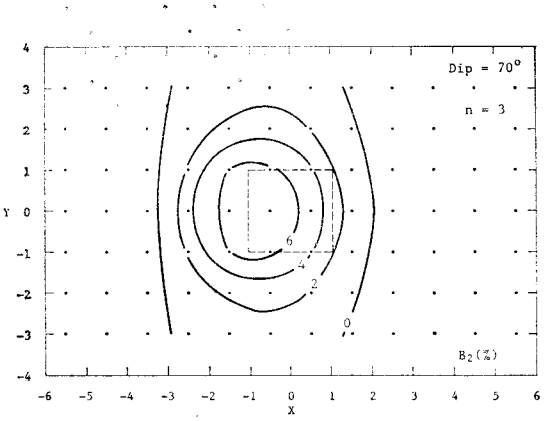

Fig. 11 IP map for the 70-degree dipping structure at n=3. The model is the same as in Fig. 10.

90-degree dip

Fig. 12 shows IP pseudo-sections over the vertical structure of 90 degrees. The width and thickness of body are 0.5 and 5 units, respectively.

In the pseudo-section at Y=0, the highest IP

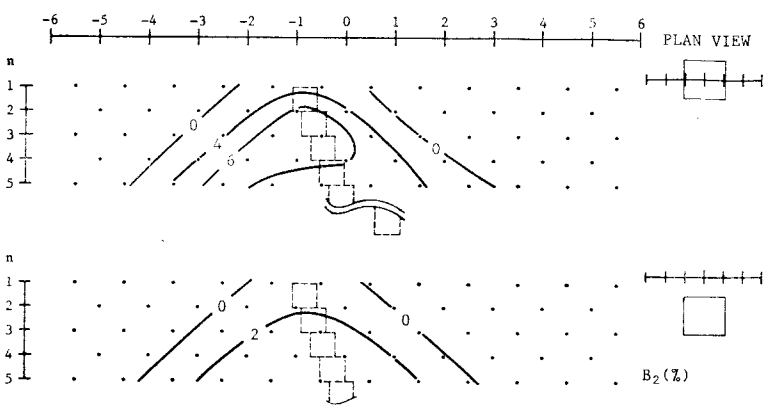

Fig. 10 IP pseudo-sections for the 70-degree dipping structure along lines Y=0 (upper) and Y=2 (lower), The total width of body is about 2.14 units, the strike length 2, the total thickness 5,the depth 1 and the resistivity ratio ρ_2/ρ_1=3.0/12.5.

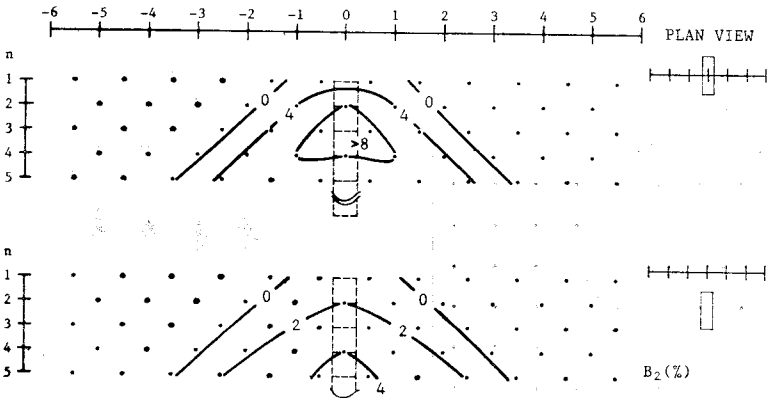

Fig. 12 IP pseudo-sections for the vertical structure along lines Y=0 (upper) and Y=2 (lower). The witdh of body is 0.5 unit, the strike length 2, the thickness 5, the depth 1 and the resistivity ratio ρ_2/ρ_1=3.0/12.5.

response over 8% appears at the upper side of body. The IP pattern is of course symmetrical. The position of anomaly is depressed by moving the line away from the center of the body. The highest IP response over 4%, for example, appears at the central part of body at Y=2.

Fig. 13 shows an IP map at n=3 over the vertical structure. Circular contours represent the location of body well.

Discussion and Conclusions

Since the dipole-dipole array is symmetrical, the effect of dip is recognized by the asymmetrical pattern of IP responses. In the case of limited strike length (3-D body) that is considered here, however, the asymmetrical pattern in the pseudo-section is usually lost when the IP line moves away from the center of the body. Only the 20-degree dipping body has the detectable asymmetrical pattern at one unit off the end of the body (Fig. 5). If the dip angle of target is deeper than 45 degrees, it will be difficult to estimate the dip angle in the actual field situation. Coggon (1973) noted the same lack of dip resolution for the dipole-dipole array even for 2-D bodies. He showed that the gradient array produces more reliable information of dip. However the gradient array will give rise to other problems such as EM coupling.

The asymmetrical pattern also appears in the IP maps for the dipping structures. As the dipole separation becomes large, in general, IP anomalies grow larger toward the direction of down-dip than toward that of up-dip. These analyses, however, may be too sophisticate for the dipping structures, except for the 20-degree dip (Figs. 6 and 7).

IP contours usually enclose the location of body in the maps at large dipole separation. Thus the IP maps are more useful than the IP pseudo-sec-

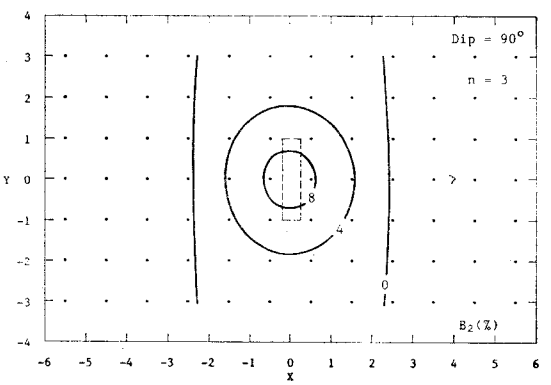

Fig. 13 IP map for the vertical structure at n=3. The model is the same as in Fig. 12.

tions in identifying the location of target. Note that, when the width of body is much longer than the thickness and the dipole separation is large, high anomalies appear separately at the both end-sides of body as shown in Figs. 4 and 7.

IP field data usually consist of both anomalies associated with targets and EM couplings. Because the EM coupling usually increases as the dipole separation becomes large (Kaku, 1966; Dey and Morrison, 1973; Hohmann, 1973), an IP pseudo-section involves the different level of the EM coupling at each dipole separation. An IP map, on the other hand, consists of the nearly same level of the EM coupling. This fact will give great benefits to more accurate interpretaion of IP field data. Note that our numerical results do not involve the EM coupling.

Acknowledgments

This research has been supported by the Korean Science and Engineering Foundation; this support is gratefully acknowledged.

References

Coggon, J. H., 1973: A comparison of IP electrode arrays, Geophysics, **38** (4), 737–761.

Dey, A. and H. F. Morrison, 1973: Electromagnetic coupling in frequency and time-domain induced polarization surveys over a multilayered earth, Geophysics, **38** (2), 380–405.

Endo, G., Y. Yamamoto, M. Takeuchi and K. No-guchi, 1979: On the numerical caluculation method using an integral equation solution (I), Butsuri-Tanko, **32** (3), 117–125. (in Japanese)

Hohmann, G. W., 1973: Electromagnetic coupling between grounded wires at the surface of a two-layer earth, Geophysics, **38** (5), 854–863.

———, 1975: Three-dimensional induced polarization and electromagnetic modeling, Geophysics, **40** (2), 309–324.

Kaku, H., 1966: On the coupling effect in the induced polarization method, Butsuri-Tanko, **19** (4,5), 168–175. (in Japanese)

Kim, H. J., 1983: Three-dimensional standard curves in induced polarization method, Jour. Korean Inst. Mining Geol., **16** (4), 269–276.

Pelton W. H., L. Rijo and C. M. Swift, Jr., 1978: Inversion of two-dimensional resistivity and induced-polarization data, Geophysics, **43** (4), 788–803.

Pridmore, D. F., G. W. Hohmann, S. H. Ward and W. R. Sill, 1981: An investigation of finite-element modeling for electrical and electromagnetic data in three dimensions, Geophysics, **46** (7), 1009–1024.

경사구조에 대한 쌍극자 IP 응답의 해석

김 희 준

요약 : 유도 분극법에서 지하의 경사 물체에 대한 3차원 표준곡선을 해석하였다. 이들 물체 대한 쌍극자 IP 응답은 적분 방정식을 이용한 수치계산 방법으로 구해졌다. 이때 물체의 경사각은 각각 0,20. 45, 70 및 90도 이다.

물체가 수평(경사각 0도) 및 수직(경사각 90도)일 때는 단면도에서 대칭성 IP 패턴이 되지만, 20, 45 및 70도로 경사하고 있을 때는 최대값의 등치선이 물체의 경사 방향과 반대 방향으로 기울어져 있는 비대칭성 패턴을 나타낸다. 이중 가장 현저한 비대칭성 패턴은 20도 경사 모델에서 나타났다. 쌍극자 IP 데이터로서 70도 경사물체와 수직물체를 식별하기는 어렵다. 또한 측선이 물체의 중심에서 주향방향으로 멀어질 때의 반응은 IP anomaly가 작은 값으로 단면도에서 보다 깊은 곳에 나타나게 된다. 한편, 탐사대상물의 위치를 추정할 때 평면도는 단면도보다 유용할 것으로 생각된다.